Photofragmentation Dynamics of *n*-Dodecanethiol-Derivatized Silver Nanoparticles in Cyclohexane

Chil Seong Ah, Hyouk Soo Han, Kwan Kim, and Du-Jeon Jang*

School of Chemistry, Seoul National University, Seoul 151-742, Korea

Received: May 5, 2000; In Final Form: June 19, 2000

Photochemical reaction of *n*-dodecanethiol-derivatized silver nanoclusters dispersed in cyclohexane has been studied in the picosecond−second time range and has been found to depend nonlinearly on the irradiance of photolysis light. The static absorption bleach by excitation at 532 and 355 nm increases with the irradiance raised to the powers of 1.9 and 1.4, respectively. Furthermore, transient absorption produced with a high-energy pulse rises further on a time scale of a few nanoseconds, whereas that with low-energy pulse decays. Transient absorption owing to the dielectric change of the immediately surrounding medium arises in 0.5 ns with the conduction of the thermalized photon energy. It decays in 1.4 ns as the heat spreads further. A fraction of excited nanoparticles experience a further absorption increase as hot alkanethiols dissociate for a period determined by the heat dissipation time (3.6 ns). The fraction increases with excitation-pulse energy. Within the recombination time (40 ns) of thiols, some dethiolated particles are also subject to fragmentation. Absorption bleach caused by disintegration recovers partially with a time constant of 0.13 s, as the fragments reassemble.

Introduction

Nanoparticles have a variety of unique spectroscopic, electronic, and chemical properties that arise from their small sizes and high surface/volume ratios.[1−4] In particular, noble-metal clusters and colloids with nanometer dimensions have attracted a great deal of interest recently. The quantum size effect, nonlinear optical effect, and electron dynamics of noble-metal nanoparticles are being extensively investigated, because they can be applied in catalysts, sensors, drug delivery, optoelectronics, and magnetic devices.[5−11] Nanoparticles also exhibit new optical properties,[1,2,12−14] which are observed neither in molecules nor in bulk metals. One particular example is the presence of a strong absorption band in the visible region, due to the surface-plasmon-oscillation modes of conduction electrons which are coupled through the surface to external electromagnetic fields. Because of this plasmon band, the optical properties of platinum, palladium, silver, and gold colloidal nanoparticles have received considerable attention.[3,4,15−29] The color of noble-metal nanoparticles is known to depend on both the size and the shape of the particles, as well as the refractive index of the surrounding medium.[12] In the region of intrinsic size, in contrast to extrinsic size, the absorption band becomes broader and the maximum absorbance decreases as the average particle size decreases.[1,4,30] The plasmon-absorption spectrum also depends significantly on the nature and concentration of adsorbed species.[28,29,31]

Many studies on colloidal nanoparticles have focused on the control of their sizes, shapes, and growth kinetics as well as on the characterization of their chemical and physical properties.[3,15−17,32−44] Nanoparticles are commonly derivatized or stabilized with organic molecules to modify their physical and chemical properties, such as their solubility, stability, and luminescence.[11,45] For example, derivatization of metal nanoparticles with alkanethiols can occur by forming a covalent bond between the sulfur atom of the alkanethiol and the surface of the particles or by chemisorption with electron-density donations from the thiolate functional group to the metal. Dry alkanethiol-derivatized silver nanoparticles are a fine brown powder and dissolve well in organic solvents such as cyclohexane to give a strong plasmon-absorption band at 440 nm.

Some types of noble-metal nanoparticles are reported to undergo optical or thermal shape transformation.[16,36,37] The laser-induced size reduction and shape change of gold nanoparticles in water have been explained to occur via melting and vaporization.[15,16] In addition, energetically unstable gold nanorods are reported to undergo thermal decomposition as well as photothermal melting and fragmentation.[35,46] While gold nanoparticles undergo physical shape transformations, silver nanoparticles are known to undergo photofragmentation following photochemical reaction.[3,47] Photoexcited silver nanoparticles suspended in water are reported to eject electrons before disintegration.[3] On the other hand, physical shape transformation via melting and vaporization occurs in *n*-alkanethiol-derivatized noble-metal nanoparticles, although the effect is less apparent for silver because of more notable fragmentation.[47] While the fragmentation efficiency decreases drastically for gold, it also lessens significantly with more-polar solvents or longer alkanethiol chains.[47]

In this paper, we report the mechanism of the photophysical relaxation and photochemical reaction of *n*-dodecanethiol-derivatized silver nanoparticles dispersed in cyclohexane. The nonlinear increase of photofragmentation efficiency with excitation irradiance is found to result from an increased contribution of dethiolation, which is a prerequisite to fragment, as compared with heat dissipation.

* Corresponding author. E-mail: djjang@plaza.snu.ac.kr.

10.1021/jp0017083 CCC: $19.00
Published on Web 08/08/2000

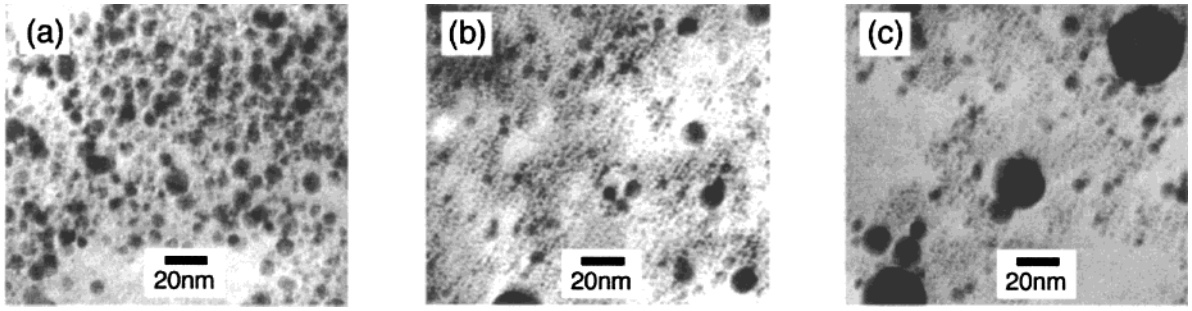

Figure 1. TEM images of $Ag_x-SC_{12}H_{25}$ nanoparticles after irradiating the nanoparticles dispersed in cyclohexane with a 40-mW beam of 355 nm and 30-ps laser pulses for 0 (a), 3 (b), and 9 (c) min.

Experimental Section

Materials. Samples of *n*-dodecanethiol-derivatized silver ($Ag_x-SC_{12}H_{25}$) nanoparticles were prepared via a two-phase synthetic route.[45] A 30-mL aqueous solution of 3×10^{-2} M $AgNO_3$ and 50 mL toluene solution of 5×10^{-2} M *n*-hexadecanesulfonic acid were poured together into a separating funnel and shaken vigorously. A 0.2-mL of neat *n*-dodecanethiol and then 25 mL of 0.4 M $NaBH_4$ aqueous solution were dropped to the separated organic phase, with stirring, over 1 h. The mixture was stirred further for 2 h, concentrated to a 10-mL solution using a rotary evaporator, diluted 20 times with ethanol, and then kept in a refrigerator at 18 °C for 4 h. Thereafter, the solution was dried using an aspirator to yield a powder, which was washed several times with toluene, ethanol, and then acetone. The powder was freshly dissolved in cyclohexane just before measurements. The typical concentration of $Ag_x-SC_{12}H_{25}$ nanoparticles and their experimentally determined extinction coefficient at the plasmon-absorption maximum were $10^{-8}-10^{-9}$ M and $10^{8}-10^{9}$ M^{-1} cm^{-1}, respectively. All the measurements were performed at room temperature.

Static Measurements. A drop of the colloid sample was applied to a carbon-coated copper grid for transmission electron micrographic (TEM) examination. Particle sizes were determined from photographs taken with a transmission electron microscope (JEOL, JEM2000). Absorption spectral changes with photolysis were monitored by measuring the absorption spectra of a 3-mL sample contained in a quartz cell having a 10-mm path length at scheduled intervals using a UV/vis spectrophotometer (Sinco, UVS2040). These measurements were performed while irradiating the sample with 30-ps pulses from a mode-locked Nd:YAG laser (Quantel, YG501) run at 10 Hz. The spot diameter of the laser beam was 8 mm at the sample.

Kinetic Measurements. Picosecond transient-absorption kinetic profiles were measured by using the above laser and a 10-ps streak camera (Hamamatsu, C2830) with a CCD (Princeton Instruments, RTE128H). The principles of the picosecond transient-absorption spectrometer utilizing dye emission and a streak camera were previously described in detail.[48] Transient absorption produced by a 355-nm excitation pulse of 2-mm spot diameter was probed using the fluorescence from an organic dye excited by a laser pulse split from the sample excitation pulse. The comparison of dye-emission kinetic profiles without and with sample excitation yields a picosecond transient-absorption kinetic profile. Nanosecond time-resolved transient-absorption spectra and kinetic profiles were obtained by exciting a sample using 6-ns pulses of 3-mm spot diameter from a Q-switched Nd:YAG laser (Quanta System, HYL101) and by monitoring the intensity changes of a 300-W Xe lamp (Schoeffel, LPS255) beam passing through the sample. The probe beam was collected into a 0.5-m spectrometer (Acton Research, Spectrapro500) coupled with an intensified CCD (Princeton Instruments, ICCD576G) having a 2-ns gate. The laser and the intensified CCD were triggered by variable delays using a pulse/delay generator (Stanford Research Systems, DG535).

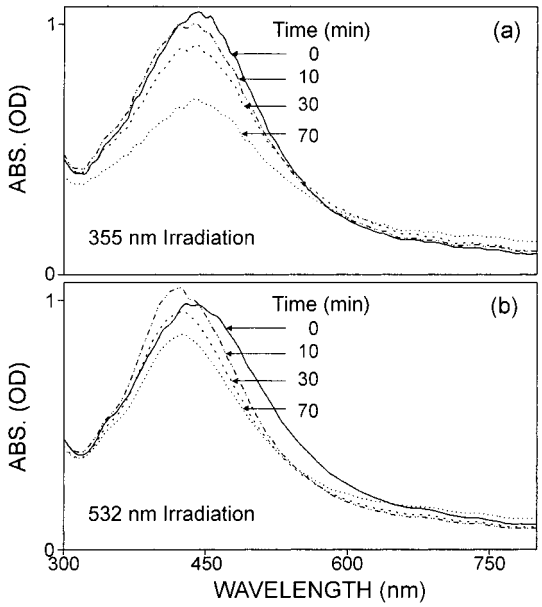

Figure 2. Absorption spectral changes of $Ag_x-SC_{12}H_{25}$ nanoparticles in cyclohexane by irradiation at 355 (a) and 532 nm (b) using a 12-mW beam of 30-ps pulses for different times.

Results and Discussion

The TEM image in Figure 1a shows that the $Ag_x-SC_{12}H_{25}$ nanoparticles as prepared are quite homogeneous in size, with an average diameter of ~6.2 nm, and are polyhedral, rather than spherical. Infrared spectral features[22] indicate that the alkyl chains are extended from the silver surface in a trans-zigzag conformation.[49] The TEM images (Figure 1b,c) show that upon irradiation, some nanoparticles dispersed in cyclohexane decompose into smaller particles and then subsequently aggregate to form even larger particles. Specifically, upon irradiation, the nanoparticles decompose into fragments smaller than 2 nm in diameter, and the overall size distribution becomes wider. Much larger particles with diameters up to 20 nm or so are formed with longer irradiation. The photochemical decomposition of the silver nanoparticles can also be seen in the UV/vis absorption spectroscopy. As shown in Figure 2, the plasmon-absorption band becomes weaker and broader upon irradiation; however, the spectral change is more significant with 355-nm irradiation than with 532-nm irradiation.

Figure 3 shows that the absorbance change of the plasmon band is dependent on the monitoring wavelength as well as the photolysis wavelength. The absorbance at the peak of the

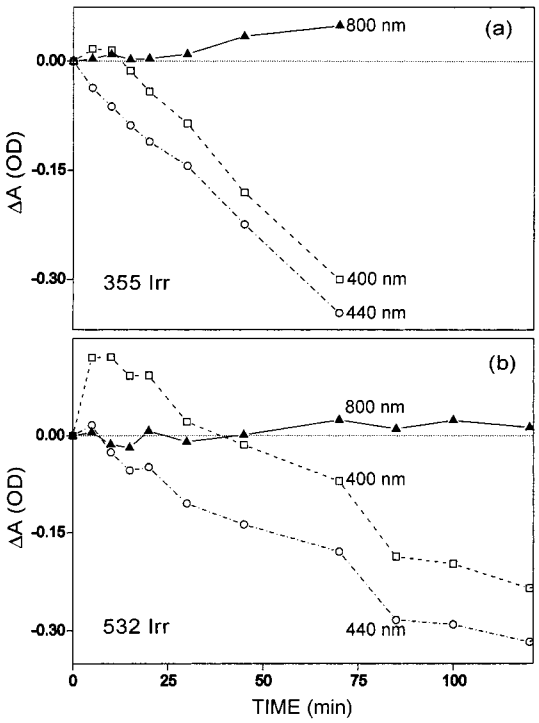

Figure 3. Absorbance changes with time of $Ag_x-SC_{12}H_{25}$ nanoparticles in cyclohexane at three wavelengths after irradiation at 355 (a) and 532 nm (b) using a 12-mW beam of 30-ps pulses.

plasmon band (440 nm) monotonically decreases upon irradiation with 355- or 532-nm light. This can be understood by invoking the fact that the plasmon absorption decreases in magnitude and becomes broader as the nanoparticles become smaller than the intrinsic-size region.[4] (The intrinsic-size region for metal nanoparticles is known to be below ~10 nm in radius, according to the Mie theory.[4,30]) On the other hand, the absorbance at a very long wavelength, that is, 800 nm, increases with the irradiation time, albeit the absorbance rises slowly with some time delay from the start of irradiation. When we consulted the literature,[35,40] we found that absorption growth at 800 nm is attributable to the longitudinal transition of enlarged eccentric nanoparticles, which can be formed from the aggregation of fragments, as well as to the broader scattering of small fragments. The particles formed by photolysis are presumed to be very polydisperse, with a wide distribution of sizes and shapes.

In contrast to the absorbances at 440 and 800 nm, the absorbance at 400 nm initially increases upon the laser irradiation, but with further irradiation it decreases. This phenomenon is more easily observable with 532-nm excitation. These absorbance changes at 400 nm seem to indicate that the fragmentation of the nanoparticles does not occur simply via a one-step shattering process but instead proceeds via a stepwise and gradual fragmentation process yielding small final sizes. Presumably in the early irradiation time, the maximum of the plasmon absorption band shifts to the blue due to the size reduction of the nanoparticles. Further irradiation leads to the formation of much smaller particles in the intrinsic-size limit, as well as to aggregated particles, thereby resulting in the gradual decrease of the plasmon absorbance at 400 nm.

The plasmon-absorption change of $Ag_x-SC_{12}H_{25}$ nanoparticles in cyclohexane is nonlinearly dependent on the intensity of the photolysis-laser light. For example, as shown in Figure 4, the absorbances at 440 and 650 nm nonlinearly decrease and increase, respectively, with irradiance increase. Bearing in mind

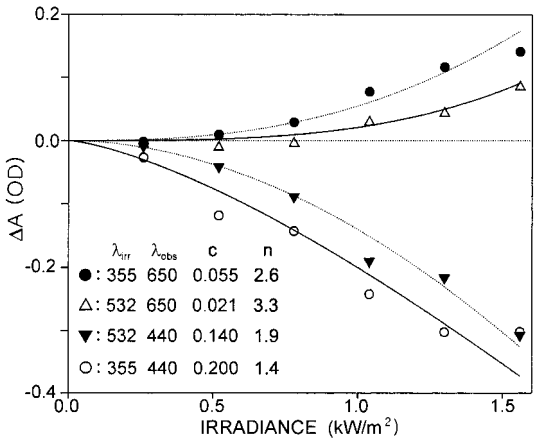

Figure 4. Irradiance-dependent absorbance changes of $Ag_x-SC_{12}H_{25}$ nanoclusters in cyclohexane. Absorption changes were measured after irradiating the samples with a 30-ps laser beam for 3 min. Each profile was fitted to c(irradiance)^n, where c and n were a constant and an exponent, respectively. The irradiation (λ_{irr}) and observation wavelengths (λ_{obs}) in nm, together with c and n, are shown inside the figure.

that the irradiance dependency is subject to the probe wavelength, as well as to the photolysis wavelength, we have attempted to fit the absorbance changes in Figure 4 to a formula, where c and n are a constant and an exponent, respectively.

$$\Delta A_{\text{photol}} = c(\text{irradiance})^n \qquad (1)$$

The values of c and n obtained are included in the insert of Figure 4. The values of the exponent n are determined to be 1.4 and 1.9 for the absorbance changes at 440 nm with the irradiation at 355 and 532 nm, respectively. On the other hand, for the absorbance changes at 650 nm following excitation at 355 and 532 nm, the values of the exponent were determined to be 2.6 and 3.3, respectively. This analysis provides a valuable insight into the mechanism of the photolysis of the silver nanoparticles. First of all, $n = 1.4$, determined from the absorbance change at 440 nm under 355-nm excitation, implies that the photolysis efficiency will increase nonlinearly with increasing irradiance. The significantly larger value of 1.9 with 532-nm excitation indicates that having enough photon energy is vital for the photolysis of the silver nanoparticles. On the other hand, the fact that the value of n is as large as 3.3 at a long probe wavelength of 650 nm implies that the aggregation of fragments, as well as the decomposition into fragments, is strongly nonlinearly dependent on the irradiance of the excitation light. It is also noteworthy that the values of n at the probe wavelength of 650 nm are nearly twice as large as those at 440 nm, regardless of the excitation wavelength. This factor is consistent with the expected reaction order of a bimolecular reaction, supporting the view that the photolyzed fragments undergo recombination to produce enlarged aggregates.

The transient-absorption data in Figure 5 show the formation and decay kinetics of transient intermediates involved in the photolysis of $Ag_x-SC_{12}H_{25}$ nanoparticles suspended in cyclohexane. However, prior to analyzing these kinetic profiles, one has to ascertain how much the kinetics of transient intermediates are affected by the excitation pulse energy, because the overall photolysis efficiency has been found to depend nonlinearly on the intensity of the excitation laser (Figure 4). In fact, as shown in Figure 6, the photolysis kinetics are strongly dependent on the excitation-pulse energy, especially in the time region of a few nanoseconds after excitation. Namely, when excited using a low-energy pulse, the apparent transient-absorption feature

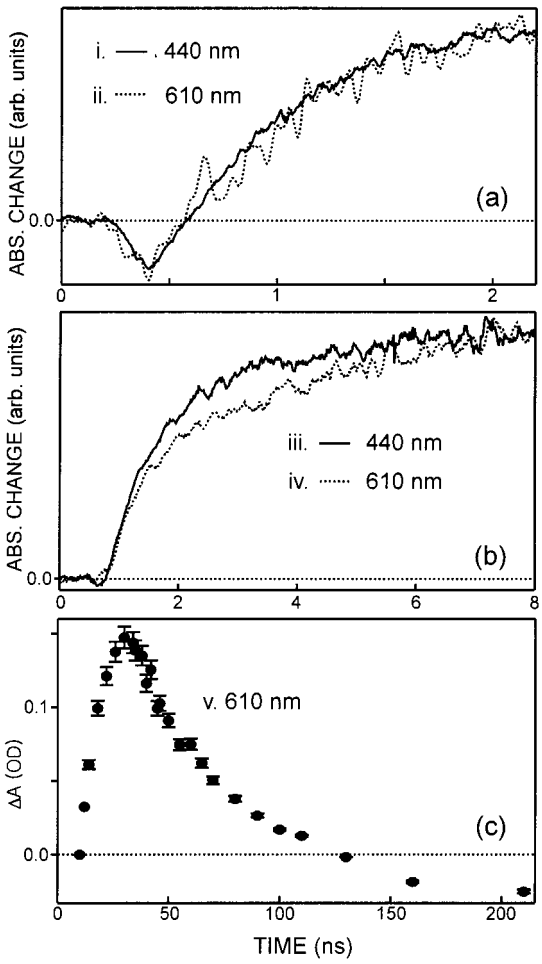

Figure 5. Transient-absorption kinetics profiles of $Ag_x-SC_{12}H_{25}$ nanoparticles in cyclohexane at various time windows. The sample was excited at 355 nm and monitored at the indicated wavelengths. The profiles in panels a and b were excited using 0.5-mJ pulses of 30-ps duration and monitored using a dye fluorescence beam using a streak camera with a 10-ps resolution, while the profile in panel c was excited using 2.1-mJ pulses of 6-ns duration and monitored using a Xe-lamp beam using a CCD with a 2-ns gate.

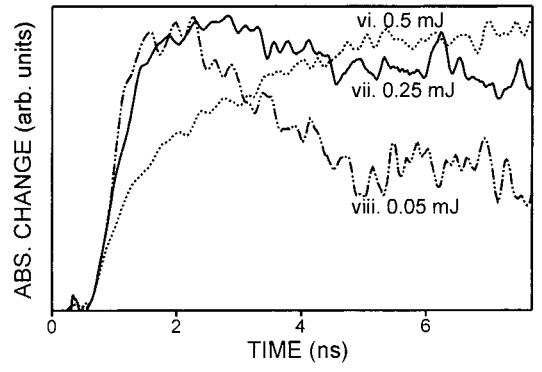

Figure 6. Excitation-energy-dependent transient-absorption kinetic profiles, measured using the streak camera, of $Ag_x-SC_{12}H_{25}$ nanoparticles in cyclohexane. The sample was excited at 355 nm and probed at 580 nm.

decays in a few nanoseconds (see profile viii in Figure 6). On the other hand, at high-energy excitation it rises continuously (profile vi). However, it is intriguing that the superficial kinetics of the fast-decay component at the low-excitation energy (profile viii) is faster than the slow-rise component at the high-excitation energy (profile vi). If high photon energy opens a new process that competes with the process that gives the decay at low energy, then the decay time of the fast component in profile viii would be expected to be longer than the formation time of the slow component in the profile vi. This is in contrast with the actual observation.

TABLE 1: Transient-Absorption Kinetic Constants[a] Extracted from Figures 5 and 6

profile	λ_{pr} (nm)	Δt_{ex} (ps)	$E_{ex}/(\pi r^2)$ (mJ π^{-1} mm^{-2})	time constant (ns) τ_{r1}	τ_{d1} (A_1)	τ_{r2} (A_2)	τ_{d2}	A_3
i	440	30	0.5/1[2]	0.5	1.4 (0.32)	3.6 (0.68)	40	−0.11
ii	610	30	0.5/1[2]	0.5	1.4 (0.32)	3.6 (0.68)	40	−0.11
iii	440	30	0.5/1[2]	0.5	1.4 (0.44)	3.6 (0.56)	40	
iv	610	30	0.5/1[2]	0.5	1.4 (0.34)	3.6 (0.66)	40	
v	610	6000	2.1/1.5[2]	0.5[b]	1.4 (0.21)	3.6 (0.79)	40	−0.08
vi	580	30	0.5/1[2]	0.5	1.4 (0.36)	3.6 (0.64)	40	
vii	580	30	0.25/1[2]	0.5	1.4 (0.66)	3.6 (0.34)	40	
viii	580	30	0.05/1[2]	0.5	1.4 (0.81)	3.6 (0.19)	40	

[a] Kinetic constants were extracted by fitting all the kinetic profiles to the same function of $\{(1-\exp(-t/\tau_{r1})\}[A_1\exp(-t/\tau_{d1})+A_2\{(1-\exp(-t/\tau_{r2})\}\exp(-t/\tau_{d2})]+A_3$ convoluted with the respective instrument-response functions. The deconvolution was iteratively repeated until all the time constants except the relative amplitudes became the same, regardless of kinetic profiles. [b] Actually, 0.5 ns was used as τ_{r1} to fit the kinetic profile measured with Δt_{ex} of 6 ns, instead of its being extracted from the profile.

Considering that the above two processes can occur simultaneously at any excitation-pulse energy, we have attributed the apparent variation in the kinetic profiles in Figure 6 to the variation of the relative contributions of the two processes, which depend on the irradiance of the excitation light. On these grounds, all the kinetic profiles in Figures 5 and 6 were fitted to the following function, invoking the fact that the slowly rising component decays much more slowly than the fast-decaying component.

$$\Delta A_{photol} = \{(1-\exp(-t/\tau_{r1})\}[A_1\exp(-t/\tau_{d1}) + A_2\{(1-\exp(-t/\tau_{r2})\}\exp(-t/\tau_{d2})] + A_3 \quad (2)$$

All the observed kinetic profiles were iteratively fitted to eq 2 convoluted with the appropriate instrument response functions until all the time constants except the relative amplitudes became the same, irrespective of the kinetic profiles. The decay constants obtained from this analysis are given in Table 1.

The negative value of A_3 in the fast-time domain of Figure 5a is attributable to the incomplete recovery of the absorption bleach produced by laser excitation. Although the bleach-recovery kinetics are too fast to measure properly with our temporal resolution, they must be related to early processes such as the thermalization of the plasmon-excitation energy via electron−phonon coupling.[2] These processes are typically complete within 10 ps. On this basis, we attribute the fast formation time of 0.5 ns to the conduction of the excitation energy to the immediately surrounding medium. It is proposed that the dielectric constant around the silver particles changes due to heating, which modifies the extinction coefficient of the nanoparticles, giving rise to a transient-absorption signal. The fast-decay component of 1.4 ns can be subsequently attributed to the relaxation of the refractive-index transient by further heat spread.

On the other hand, the slow-formation component with the time constant of 3.6 ns is assigned to dissociation of thiols from the silver surface. The resulting nanoparticles will have a net positive charge and, thus, a different absorption spectrum from that of the initial neutral particles.[24] Mulvaney[24] has reported that a decrease in the particle electron density enhances the surface-plasmon absorbance of silver nanoparticles in the wavelength region >400 nm. Kamat et al.[3] have also attributed

the transient-absorption rise of 1.5 ns at 600 nm to the photoejection of electrons from the silver nanoparticles suspended in water. These previous reports indicate that the transient-absorption rise time of 3.6 ns is at least related to a decrease in the particle electron density. In addition, we[47] have reported that the rise time becomes larger with longer alkanethiol. Considering this and the fact that our rise time is longer than the electron-ejection time,[3] we attribute the 3.6-ns transient-absorption rise to dethiolation. It is noteworthy that the dissociation of a thiol from the silver surface or the reduction of a thiol is less unfavorable energetically than the oxidation of silver.[50] Thus, if the silver surface ejects an electron, a thiol group accepts the electron to become a thiolate ion. In other words, dethiolation favors the photoejection of electrons from the particles energetically but it retards the ejection process kinetically. One can say that the formation of the thiolate ion in nonpolar cyclohexane will be unfavorable. In this regard, we suggest that dethiolation is a process of electron charge-density shift from the silver to the thiol to form a thiolate ion-adsorbed silver nanoparticle.[28]

While the transient kinetics in Figure 5a, measured at two different probe wavelengths, are comparable to each other, those in Figure 5b are slightly different. This can be understood by simply assuming that the absorption spectrum of the slow-rising transient is different from that of the fast-decaying component. The decay time of 40 ns in Figure 5c is attributable in turn to the recombination time for the dissociated thiolates with the silver surface. The reduction of the transient absorption below zero in Figure 5c is consistent with the decrease of the static-plasmon absorption by photolysis in Figure 2 and indicates that some of the dethiolated nanoparticles experience fragmentation, as shown by the TEM images in Figure 1. Considering the much smaller bleach amplitude relative to the transient absorption in Figure 5c, we believe that the rate constant of disintegration should be much smaller than the inverse of the recombination time (40 ns).

The relative amplitude of the slow-rising transient is also dependent on the intensity of the excitation-laser light (Figure 6). The fast decay time of 1.4 ns and the slow rise time of 3.6 ns are reported[47] to be the same for *n*-dodecanethiol-derivatized gold and composite silver/gold nanoparticles suspended in the same solvent. However, the relative amplitude of the slow-rising transient decreases in those particles, especially for gold. These facts indicate that the rise time of 3.6 ns is the time necessary for the derivatizer to reach a threshold thermal level, below which dethiolation cannot occur. This then suggests that the dethiolation rate constant is in fact much smaller than the heat dissipation rate constant of $(3.6\ \text{ns})^{-1}$. It is our belief that although both times are determined by the same heat-dissipation process, the rise time (3.6 ns) for the transient corresponding to dissociation is longer than the relaxation time (1.4 ns) of the artificial nonlinear refractive-index transient. Then the question will arise why two phenomena determined by the same process have different time constants. The refractive-index transient decays as the heat in the immediately surrounding medium, such as sulfur atoms, spreads over the alkanethiol chains. However, dethiolation is suggested to occur as a result of alkanethiol thermal motion. Thus, it can occur until the chains lose the thermal energy to reach the threshold level. Apparently, the variation of dethiolation possibility with the variation of the excitation irradiance alters the overall transient-absorption kinetic feature in the time range of several nanoseconds (Figure 6).

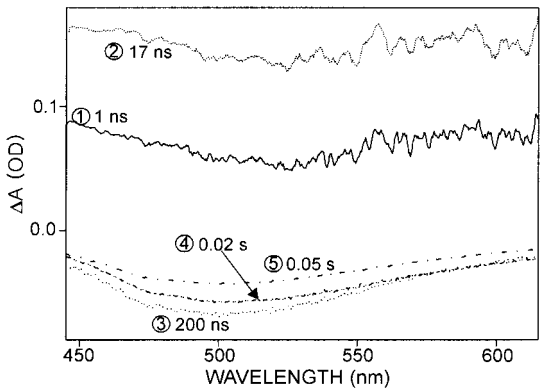

Figure 7. Time-resolved transient-absorption spectra of $Ag_x-SC_{12}H_{25}$ nanocrystals in cyclohexane at various delay times (shown inside) after excitation with 3-mJ, 355-nm laser pulses of 6-ns duration.

It is then quite intriguing to understand why a high irradiance enhances the fraction of the dethiolation channel. A simple calculation shows that a nanoparticle at the experimental conditions of Figure 6 absorbs 10^3-10^4 photons on average from a single excitation laser pulse of 30-ps duration. Because the thermalization of plasmon-excitation energy via electron−phonon coupling is reported to occur within 10 ps,[2] all the absorbed photons (N in a particle) are converted into heat within the pulse duration time of 30 ps. Because a fraction (f) of this thermalized photon energy ($N\epsilon_{h\nu}$) is contained in the thiols at a given time, the transient absorbance arising from dethiolation ($\Delta A_{\text{dethiol}}$) can be related to the following equation, where E_{th} is the threshold thermal energy level for dethiolation.

$$\Delta A_{\text{dethiol}} \propto \exp\{-E_{\text{th}}/(fN\epsilon_{h\nu})\} \tag{3}$$

It is assumed in eq 3 that only the dodecanethiols with the heat ($fN\epsilon_{h\nu}$) greater than E_{th} can undergo dissociation. As will be shown below, the increase of $\Delta A_{\text{dethiol}}$, as well as the variation of the apparent kinetic feature with the excitation light irradiance, can be understood from eq 3.

Because the chance of disintegration, as well as the static-absorbance change resulting from disintegration (ΔA_{photol}), in Figure 4 is proportional to $\Delta A_{\text{dethiol}}$, we can write a new equation by combining eqs 1 and 3.

$$\Delta A_{\text{photol}} \propto \Delta A_{\text{dethiol}} \propto (\text{irradiance})^n \propto \exp\{-E_{\text{th}}/(fN\epsilon_{h\nu})\} \tag{4}$$

It is interesting to note that as the excitation wavelength changes from 355 to 532 nm, the n observed at the probe wavelength of 440 nm increases by a factor similar to the energy ratio, r, of a 355-nm photon to a 532-nm photon. If the $\epsilon_{h\nu'}$ in eq 4 is $\epsilon_{h\nu}/r$, ΔA_{photol} becomes proportional to $\exp\{-E_{\text{th}}/(fN\epsilon_{h\nu})\}^r$. This explains qualitatively why the exponent of eq 1 increases with a longer wavelength excitation. The observed exponent of <2 at both excitation wavelengths is not the number of photons necessary to satisfy E_{th}. It rather suggests that the nanoparticles that absorb more photons have a greater chance of undergoing fragmentation. Thus, fragmentation occurs both thermally and statistically.

A series of time-resolved transient-absorption spectra have been recorded to show the progressive spectral changes of the plasmon absorption after a pulsed excitation (Figure 7). All of the spectra are almost featureless, even though a hollow absorption region is clearly identified. The overall spectral features are nonetheless understood by referring to the aforementioned photoreaction mechanism. As presumed previously,

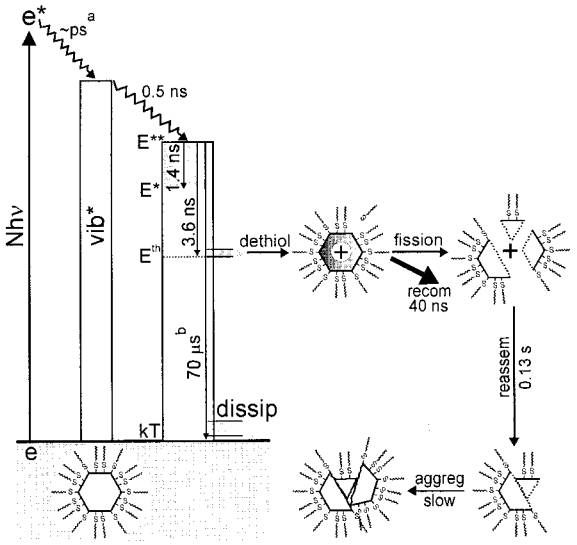

Figure 8. Schematically presented photoreaction mechanism of $Ag_x-SC_{12}H_{25}$ nanoparticles dispersed in cyclohexane. The degree of shading symbolically represents the relative extent of absorbance at each stage. The times for thermalization[a] and thermal relaxation[b] are cited from refs 2 and 16, respectively.

the positive transient absorption at 1 ns can be related to the refractive-index transient of the alkyl chains caused by conduction of the thermalized photon energy. The further-enhanced positive absorbance at 17 ns is ascribed to the dethiolated nanoparticles that form in the time scale of 3.6 ns. The decrease in the absorption hollow near 530 nm at 17 ns, compared with that at 1 ns, also supports the suggestion that the slight difference between the profiles iii and iv in Figure 5 is due to the slight spectral difference between the slow- and fast-rising transients. As the dissociated thiols recombine to the silver surface in 40 ns, the transient absorbance decreases in all spectral regions. The spectrum at the delay time of 200 ns is absorption bleach rather than transient absorption. Such absorption bleach is associated with the formation of the fragmented nanoparticles. The blue shift of the hollow absorption region at 200 ns is also attributable to fragmentation. The absorption bleach recovers slowly, with a time constant of 0.13 s, as the fragmented nanoparticles reassemble, owing to the reduced solubility of the newly exposed thiolate-free sides. The absorption bleach at 0.05 s in Figure 7 is much broader and more red-shifted than the static-absorbance changes by photolysis in Figure 2. This indicates that the recombination of fragments or a further aggregation of the agglomerates takes place continuously by a much slower rate. As evidenced from Figure 2, the bleach never recovers completely, even after an infinite period of time. The fragmentation into much smaller particles and/or the aggregation into much larger particles will reduce the overall plasmon absorption.

Figure 8 summaries schematically the mechanism of the photophysical relaxation and photochemical reaction of $Ag_x-SC_{12}H_{25}$ nanoparticles dispersed in cyclohexane. Static-absorption bleach by excitation at 532 and 355 nm increases with the irradiance raised to the powers of 1.9 and 1.4, respectively. Furthermore, transient absorption produced with a high-energy pulse rises farther on a time scale of a few nanoseconds, but it decays with a low-energy pulse. Transient absorption arises within 0.5 ns, owing to the dielectric change of the derivatizer induced by heating. Physical shape transformations via melting and vaporization are also considered to occur until the heat conduction time,[16,47] although the evidence is erased by the severe fragmentation. While the dielectric transient decays in 1.4 ns, a fraction of excited nanoparticles experience a further absorption increase as the hot alkanethiols dissociate, with a time constant of 3.6 ns. The relative importance of dethiolation, as compared with heat dissipation, increases with excitation-pulse energy. This variation causes the apparent transient-absorption kinetics to change, as well as a nonlinear increase in the photolysis efficiency. Some of dethiolated particles are also subject to fragmentation within the recombination time of 40 ns. The transient bleach produced by disintegration recovers partially, with a time constant of 0.13 s, as fragments reassemble, owing to their reduced solubility. Although much slower aggregation follows endlessly, the bleach never recovers completely.

Acknowledgment. We thank the Center for Molecular Catalysis and the Basic Research Science Institute Program for financial support. C.S.A. and H.S.H. also thank the Brain Korea 21 Program for a fellowship.

References and Notes

(1) Alvarez, M. M.; Khoury, J. T.; Schaaff, T. G.; Shafigullin, M. N.; Vezmar, I.; Whetten, R. L. *J. Phys. Chem. B* **1997**, *101*, 3706.
(2) Hodak, J. H.; Martini, I.; Hartland, G. V. *J. Phys. Chem. B* **1998**, *102*, 6958.
(3) Kamat, P. V.; Flumiani, M.; Hartland, G. V. *J. Phys. Chem. B* **1998**, *102*, 3123.
(4) (a) Logunov, S. L.; Ahmadi, T. S.; El-Sayed, M. A.; Khoury, J. T.; Whetten, R. L. *J. Phys. Chem. B* **1997**, *101*, 3713. (b) Link, S.; El-Sayed, M. A. *J. Phys. Chem. B* **1999**, *103*, 8410.
(5) Schmid, G.; West, H.; Mehles, H.; Lehnert, A. *Inorg. Chem.* **1997**, *36*, 891.
(6) Nashner, M. S.; Frenkel, A. I.; Adler, D. L.; Shapley, J. R.; Nuzzo, R. G. *J. Am. Chem. Soc.* **1997**, *119*, 7760.
(7) Boal, A. K.; Rotello, V. M.; *J. Am. Chem. Soc.* **1999**, *121*, 4914.
(8) Crooks, R. M.; Ricco, A. *J. Acc. Chem. Res.* **1998**, *31*, 219.
(9) Toshima, N.; Yonezawa, T.; Kushihashi, K. *J. Chem. Soc., Faraday Trans.* **1993**, *89*, 2537.
(10) Thomas, J. M. *Pure Appl. Chem.* **1988**, *60*, 1517.
(11) (a) Chan, W. C. W.; Nie, S. *Science* **1998**, *281*, 2016. (b) Kuno, M.; Lee, J. K.; Dabbousi, B. O.; Mikulec, F. V.; Bawendi, M. G. *J. Chem. Phys.* **1997**, *106*, 9869.
(12) Underwood S.; Mulvaney, P. *Langmuir* **1994**, *10*, 3427.
(13) Hostetler, M. J.; Zhong, C.-J.; Yen, B. K. H.; Anderegg, J.; Gross, S. M.; Evans, N. D.; Porter, M.; Murray, R. W. *J. Am. Chem. Soc.* **1998**, *120*, 9396.
(14) Link, S.; El-Sayed, M. A. *J. Phys. Chem. B* **1999**, *103*, 4212.
(15) Fujiwara, H.; Yanagida, S.; Kamat, P. V. *J. Phys. Chem. B* **1999**, *103*, 2589.
(16) Takami, A.; Kurita, H.; Koda, S. *J. Phys. Chem. B* **1999**, *103*, 1226.
(17) Hodak, J.; Martini, I.; Hartland, G. V. *Chem. Phys. Lett.* **1998**, *284*, 135.
(18) Link, S.; Mohamed, M. B.; El-Sayed, M. A. *J. Phys. Chem. B* **1999**, *103*, 3073.
(19) Link, S.; Wang, Z. L.; El-Sayed, M. A. *J. Phys. Chem. B* **1999**, *103*, 3529.
(20) Johnson, P. B.; Christy, R. W. *Phys. Rev. B* **1972**, *6*, 4370.
(21) Palpant, B.; Prével, B.; Lermé, J.; Cottancin, E.; Pellarin, M.; Treilleux, M.; Perez, A.; Vialle, J. L.; Broyer, M. *Phys. Rev. B* **1998**, *57*, 1963.
(22) Han, S. W.; Kim, Y.; Kim, K. *J. Colloid Interface Sci.* **1998**, *208*, 272.
(23) Van Der Zande, B. M. I.; Bóhmer, M. R.; Fokkink, L. G. J.; Schónenberger, C. *J. Phys. Chem. B* **1997**, *101*, 852.
(24) Mulvaney, P. *Langmuir* **1996**, *12*, 788.
(25) Reetz, M. T.; Helbig, W.; Quaiser, S. A.; Stimming, U.; Breuer, N.; Vogel, R. *Science* **1995**, *267*, 367.
(26) Henglein, A.; Ershov, B. G.; Malow, M. *J. Phys. Chem.* **1995**, *99*, 14129.
(27) Taleb, A.; Petit, C.; Pileni, M. P. *J. Phys. Chem. B* **1998**, *102*, 2214.
(28) Linnert, T.; Mulvaney, P.; Henglein, A. *J. Phys. Chem.* **1993**, *97*, 679.
(29) Strelow, F.; Henglein, A. *J. Phys. Chem.* **1995**, *99*, 11834.
(30) Kreibig, U.; Vollmer, M. *Optical Properties of Metal Clusters*; Springer: Berlin, 1995; Chapter 2.
(31) Henglein, A.; Meisel, D. *J. Phys. Chem. B* **1998**, *102*, 8364.

(32) Aizenberg, J.; Black, A. J.; Whitesides, G. M. *J. Am. Chem. Soc.* **1999**, *121*, 4500.

(33) Teranishi, T.; Hosoe, M.; Tanaka, T.; Miyake, M. *J. Phys. Chem. B* **1999**, *103*, 3818.

(34) Torigoe, K.; Esumi, K. *J. Phys. Chem. B* **1999**, *103*, 2862.

(35) Mohamed, M. B.; Ismail, K. Z.; Link, S.; El-Sayed, M. A. *J. Phys. Chem. B* **1998**, *102*, 9370.

(36) Petroski, J. M.; Wang, Z. L.; Green, T. C.; El-Sayed, M. A. *J. Phys. Chem. B* **1998**, *102*, 3316.

(37) Wang, Z. L.; Petroski, J. M.; Green, T. C.; El-Sayed, M. A. *J. Phys. Chem. B* **1998**, *102*, 6145.

(38) Chen, S.; Ida, T.; Kimura, K. *J. Phys. Chem. B* **1998**, *102*, 6169.

(39) Hornyak, G. L.; Patrissi, C. J.; Martin, C. R. *J. Phys. Chem. B* **1997**, *101*, 1548.

(40) Yu, Y.-Y.; Chang, S.-S.; Lee, C.-L.; Wang, C. R. C. *J. Phys. Chem. B* **1997**, *101*, 6661.

(41) Ahmadi, T. S.; Wang, Z. L.; Green, T. C.; Henglein, A.; El-Sayed, M. A. *Science* **1996**, *272*, 1924.

(42) Sarathy, K. V.; Raina, G.; Yadav, R. T.; Kulkarni, G. U.; Rao, C. N. R. *J. Phys. Chem. B* **1997**, *101*, 9876.

(43) Reetz, M. T.; Helbig, W. *J. Am. Chem. Soc.* **1994**, *116*, 7401.

(44) Foss, C. A., Jr.; Hornyak, G. L.; Stockert, J. A.; Martin, C. R. *J. Phys. Chem.* **1994**, *98*, 2963.

(45) (a) Kang, S. Y.; Kim, K. *Langmuir* **1998**, *14*, 226. (b) Ah, C. S.; Han, H. S.; Kim, K.; Jang, D.-J. *Mol. Cryst. Liq. Cryst.* **1999**, *337*, 209.

(46) Link, S.; Burda, C.; Mohamed, M. B.; Nikoobakht, B.; El-Sayed, M. A. *J. Phys. Chem. B* **1999**, *103*, 1165.

(47) Ah, C. S.; Han, H. S.; Kim, K.; Jang, D.-J. *Pure Appl. Chem.*, **2000**, *72*, 91.

(48) Jang, D.-J.; Kelley, D. F. *Rev. Sci. Instrum.* **1985**, *56*, 2205.

(49) Luedtke, W. D.; Landman U. *J. Phys. Chem. B* **1998**, *102*, 6566.

(50) Lee, Y. J.; Jeon, I. C.; Paik, W.-K.; Kim, K. *Langmuir* **1996**, *12*, 5830.